# Sediment transport partitioning in the swash zone of a large-scale laboratory beach

Jack Puleo[1], Thijs Lanckriet[2], Daniel Conley[3], Diane Foster[4]

[1]Corresponding author, Associate Professor, Center for Applied Coastal Research, University of Delaware, Newark, DE 19716, USA, jpuleo@udel.edu, 302-831-2440
[2]Doctoral Candidate, Center for Applied Coastal Research, University of Delaware, Newark, DE 19716, USA, thijs@udel.edu, 302-931-6550. Now at International Marine & Dredging Consultants, Coveliersstraat 15, 2600 Antwerp, Belgium
[3]Associate Professor, Plymouth University, Room 121, Reynolds, Drake Circus, Plymouth, Devon, UK, PL4 8AA, daniel.conley@plymouth.ac.uk, +441752584561
[4]Associate Professor, University of New Hampshire, Kingsbury Hall, W107, Durham, NH 03284, USA, diane.foster@unh.edu, 603-862-3089.

**Keywords**: Sheet flow, suspended sediment, swash zone, sediment flux, velocity profile

**Abstract**: Swash zone sheet flow and suspended sediment transport rates are estimated on a coarse sand beach constructed in a large-scale laboratory wave flume. Three test cases under monochromatic waves with wave heights of 0.74 m and wave periods of 8 and 12.2 s were analyzed. Sediment flux in the sheet flow layer exceeds several hundred kg $m^{-2}$ $s^{-1}$ during both uprush and backwash. Suspended sediment flux is large during uprush and can exceed 200 kg $m^{-2}$ $s^{-1}$. Instantaneous sediment flux magnitudes in the sheet layer are nearly always larger than those for suspended sediment flux. However, sediment transport rates, those integrated over depth, indicate that suspended load transport is dominant during uprush for all cases and during the early stages of backwash except in the case for the 12.2 s wave case when the foreshore was steeper. Results could not be obtained for an entire swash event and were particularly truncated during backwash when water depths fell below the elevation of the lowest current meter.

**Highlights**: 1) Sheet flow instantaneous flux estimates exceed those for suspended sediment transport. 2) Depth-integrated sediment transport is dominated by suspended load during uprush. 3) Sediment transport rates could not be estimated during the latter stages of backwash when the depth is shallower than the lowest current meter.

## 1. Introduction

Quantifying and predicting sediment transport in the swash zone continues to be a challenge for coastal engineers and scientists. The swash zone, where wave-driven flows alternately wash up and down the beach face, is challenging due to rapid, turbulent, shallow, ephemeral flows. Sediment concentrations near the bed are extremely high and occur in a thin layer whereas suspended sediment concentrations may also be large and nearly uniform throughout the water column depending on forcing conditions.

The majority of present knowledge of swash-zone sediment transport arises from field studies that focus on suspended sediment fluxes. Suspended sediment fluxes are estimated as the product of local velocity and sediment concentration (e.g. Alsina and Caceres, 2011; Butt and Russell, 1999; Masselink *et al.*, 2005; Puleo *et al.*, 2000). Given the challenges associated with sensor deployment, flux estimates are obtained at a limited number (1-3) of elevations leading to a coarse under-resolution of the vertical variability and bulk mass flux estimate. Improved vertical resolution is attainable using fiber or miniature optic backscatter sensors (FOBS or MOBS) that can yield a concentration profile at up to 0.01 m resolution (Butt *et al.*, 2009; Conley and Beach, 2003; Puleo, 2009; Puleo *et al.*, 2000). However, neither OBS nor FOBS/MOBS provide any information on sediment flux processes that occur in the high concentration lower flow region near the bed. These nearbed sediment fluxes include contributions from bed load and/or sheet flow. There may be considerable overlap between the two transport modes. The commonly assumed formulation is followed in that bed load is characterized as saltating grains whereas sheet flow is composed of an entire layer of sediment under active transport. A study on time-integrated sediment transport indicated the importance of nearbed sediment transport relative to suspended sediment transport (Horn and Mason, 1994). Other limited in situ data from the swash zone (Yu *et al.*, 1990) quantified the magnitude of the nearbed sediment concentration but flux estimates were not presented. New sensors have been designed that more fully resolve the vertical profile of sediment concentration in the sheet layer (Lanckriet *et al.*, 2013; Lanckriet *et al.*, 2014; Puleo *et al.*, 2010). Preliminary results using these sensors indicate the nearbed sediment transport is a significant fraction of the total load sediment transport (Puleo *et al.*, 2014b). Horizontal gradients in the total load sediment transport (depth-integrated bed load plus suspended load), regardless of the dominant transport mode, drive small-scale local morphological change on an inter-swash basis (Blenkinsopp *et al.*, 2010; Masselink *et al.*, 2009; Puleo *et al.*, 2014a). In an alongshore uniform environment (or assumption thereof), fluxes can also be estimated with the sediment continuity equation by measuring the morphologic change at numerous cross-shore locations (Blenkinsopp *et al.*, 2011; Masselink *et al.*, 2009). However, this inference does not quantify individually the contribution of each of the two sediment transport modes.

As mentioned previously, sediment concentration and velocity are both needed to quantify sediment flux. Sediment transport studies normally focus on the cross-shore component and utilize impeller (e.g. Puleo *et al.*, 2000), electromagnetic (e.g. Masselink *et al.*, 2005) or Acoustic Doppler Velocimeters (ADVs; e.g. Raubenheimer, 2002). Typical impellers have a diameter that does not allow for measurements in close proximity to the bed. The other two sensor types have a smaller measuring volume and can be located within just a few centimeters of the bed. Only several of these sensors can be deployed above a particular horizontal location to measure the vertical distribution of swash-zone velocity due to their size and/or measuring characteristics. Recently, a new profiling velocimeter (Craig *et al.*, 2011) has been used to quantify the vertical distribution of the nearbed velocity at high spatial resolution (0.001 m) under benign (Puleo *et al.*, 2012; Wengrove and Foster, 2014) and more energetic (Puleo *et al.*, 2012; Puleo *et al.*, 2014b) forcing conditions.

Puleo *et al.* (2014b) describe more fully the difficulty in measuring in the shallow water swash-zone flows. Of particular importance is obtaining a velocity time series throughout an entire swash event. Electromagnetic and acoustic sensors are disrupted when they are first wetted by an incoming turbulent bore. Noisy data are more problematic for the acoustic sensor due to the bubbly bore/swash front. Both sensors suffer from positional difficulties in that they are, by necessity, located some finite distance above the bed. Thus, when the backwash recedes and the swash lens thins, there will be a portion of the swash event where velocities cannot be obtained using the same current meter. This “missing” portion may represent more than half the true swash cycle duration (see Section 5) depending on hydrodynamic conditions and current meter elevation. Moreover, in particularly energetic environments, there can be more than a centimeter of morphologic change resulting in considerable variability in the relative position from the bed (Puleo *et al.*, 2014a). Every study that uses an elevated current meter will have this problem of artificially truncating the swash event unless current meter data are supplemented with other information. Ultrasonic distance meters (Turner *et al.*, 2008), LIDAR (Blenkinsopp *et al.*, 2010), or particle image velocimetry (e.g. Holland *et al.*, 2001; Puleo *et al.*, 2003a) can provide some measure of the velocity throughout the full swash cycle. The former two methods are used to quantify the depth-averaged velocity through volume continuity procedures. The latter method is able to quantify only the free surface horizontal velocity.

The flow field in direct vicinity of the bed under field conditions is unknown regardless of the location of the lowest current meter or the use of image-based velocimetry techniques. Flows in this nearbed region (order of several centimeters) are generally assumed to be either depth-uniform using the value from an elevated current meter (e.g. Puleo *et al.*, 2000) or assuming a logarithmic profile (Raubenheimer *et al.*, 2004). Recent velocity profile measurements on a moderately steep, microtidal, low energy beach (Puleo *et al.*, 2012) and a macrotidal, high energy beach (Puleo *et al.*, 2014b) indicated the existence of a logarithmic profile near the bed under much of the measured swash duration. Ruju *et al.*, (this issue) show that the shape of the nearbed velocity profile on energetic, steep, beaches is also logarithmic for much of the measured swash duration.

This paper focuses on observations of nearbed swash-zone sediment flux obtained during the BARDEX II study (Masselink *et al.*, this issue). The main emphasis of this effort is to determine the relative importance of suspended to sheet flow sediment transport. Section 2 describes the experimental details relevant to this paper. Section 3 explains the quality control procedures used on the data set and bed level identification as it varied throughout a swash cycle. Formulations for sediment concentrations and transport are given in Section 4. Section 5 provides results related to sheet flow and suspended sediment flux profiles and integrated transport rates. Ensemble-average events for the three test cases are also presented. Discussion and conclusions are given in Section 6 and Section 7 respectively.

## 2. Large-Scale Laboratory Experiment and Instrumentation

### 2.1 Set Up and Conditions

The BARDEX II experiment was conducted in the Delta Flume, the Netherlands to investigate barrier dynamics. Full experimental details are provided by (Masselink *et al.*, this issue). A right-handed coordinate system was established with $x$ increasing onshore and $z'$ vertically up. The horizontal origin is the neutral position of the wave paddle and the vertical datum for the experiment is the bottom of the wave flume. We note that the vertical coordinate is designated with a prime here because analyses throughout the paper will alter the datum for the vertical coordinate to be that of the instantaneous bed level (see Section 3). The initial beach profile consisted of: an offshore sloping section from 24-29 m up to a sediment thickness of 0.5 m, a uniform thickness section from 29-49 m, a 1:15 sloping section from 49-109 m, a 5 m wide berm crest from 109-114 m and a 1:15 landward sloping section from 114-124 m. The sediment used in the experiment was moderately sorted coarse sand with a median grain diameter of 0.43 mm. Five experiment series were conducted to investigate the different barrier morphological responses (Masselink *et al.*, this issue; Table 1). At the end of some of the tests, monochromatic wave runs were conducted providing the potential for ensemble averaging. Data from monochromatic runs following tests A2 (July 12, 2012), A4 (July 14, 2012) and A6 (July 18, 2012) are presented here because they provided the best coverage of bed load and suspended sediment transport. Reference to a particular test refers only to the monochromatic run within that test. Experimental conditions for these monochromatic cases are given in Table 1. The monochromatic wave height was 0.74 m for all three tests but the period changed from 8 s for test A2 and A4 to 12.2 s for test A6. In addition, the water level in the lagoon was higher than sea level for test A2, lower than sea level for test A4 and the same as sea level for test A6.

## 2.2 Beach Profiles

A mechanical beach profiler attached to an overhead carriage recorded the beach elevation along the flume centerline following each run within a test series. Any alongshore non-uniformity cannot be captured with the profiler. Some alongshore non-uniformity in the morphology and accompanying swash flows was observed visually for several of the runs within the A series of tests but was not routinely quantified. Figure 1 shows the original beach profile and the beach profile following each monochromatic test series described here. The beach steepened through the A series of tests with erosion in the seaward swash and berm development landward. Swash zone data discussed here were collected at a cross-shore location of $x$ = 89.6 m (vertical dashed line in Figure 1). Elevation changes at this cross-shore location are much smaller than those landward and seaward. The foreshore slope measured from 85 m < $x$ < 95 m is 1:10, 1:9.5 and 1:7 for test A2, A4 and A6 respectively. The steepness increases to 1:8.9, 1:8.7 and 1:6.5 respectively if only the local bathymetry near the sensors (89 m < x < 91 m) is considered.

## 2.3 Sensors

As mentioned in Section 2.2 only swash-zone data from the central swash-zone measurement location ($x$ = 89.6 m) are presented in this paper (Figure 2). Velocities were collected using 2 Valeport electromagnetic current meters (EMCMs) and 2 acoustic Doppler profiling velocimeters (VECs). The EMCMs measure the horizontal velocity components ($u$,$v$) only. EMCMs were separated by 0.1 m in the alongshore direction and by 0.03 m in the vertical direction. EMCM data were collected at 6 Hz. The VECs are Nortek Vectrino II sensors (Craig *et al.*, 2011) that measure a velocity profile of all 3 velocity components ($u$,$v$,$w$) at up to 0.001 m vertical resolution. VECs recorded at 100 Hz in continuous mode so that no data were lost in between a file close/open sequence. The 2 VECs were separated by roughly 0.2 m in the alongshore direction and by 0.025 – 0.03 m in the vertical direction. This separation provided a highly-resolved velocity profile over up to the lower 0.06 m of the water column. Often the range of the acoustic velocity profile bins intersected the at-rest bed level. However, under active sheet flow conditions it is not clear how far the acoustic pulse penetrates into the sheet layer. Water levels were recorded by a buried pressure transducer (Druck PTX1830) and recorded at 6 Hz.

Two different sensors were used to measure sediment concentration. Suspended sediment concentration (SSC) was recorded using 4 Campbell Scientific Optical Backscatter Sensors (OBSs) within the water column. Sensors were separated in the vertical by 0.02 m. The initial elevation of the lowest sensor varied with test number. The lowest OBS was located at 0.053 m, 0.04 m and 0.032 m at the beginning of the monochromatic forcing for tests A2, A4 and A6 respectively. OBS concentrations were recorded at 16 Hz. Sediment concentrations in the sheet flow layer were measured using a conductivity concentration profiler (Figure 2B,C) designed at the University of Delaware (CCP; for a full description see Lanckriet *et al.*, 2013; Lanckriet *et* *al.*, 2014; Puleo *et al.*, 2014b). The CCP uses electric conductivity as a proxy for sediment concentration. Water has conductivity several orders of magnitude higher than the essentially non-conductive sand. The conductivity of a particular volume in space decreases as a function of the sand/water ratio within the volume. The CCP profiles the sheet flow sediment concentrations (SFSC) with 0.001 m vertical resolution over a range of 0.029 m. The CCP consists of a removable probe with gold-plated electrodes and a PVC housing containing the electronics (Figure 2B). The actual sensing mechanism relies on the 4-electrode approach (Li and Meijer, 2005). Multiplexers within the circuitry shift the active elements through the electrode array to return the SFSC profile. Sensors were deployed by burial with only the small measurement portion with cross-sectional area of 0.0016 m (thick) x 0.0056 m (wide) x ~ 0.04 m (high) exposed to the flow (Figure 2C). Sensor burial reduces scour and wake effects and the surrounding sand helps support the thin, semi-flexible probe tip. Several CCPs were deployed under the VECs and separated in the alongshore by approximately 0.2 m. Sensors were aligned visually during deployment such that the electrodes were parallel to the cross-shore direction. CCPs were sampled at 8 Hz.

## 3. Data Quality Control and Bed Level Identification

Data from different sensors were collected on separate laptop computers. Individual computers were time synchronized to a common time datum but individual samples were not triggered simultaneously. Data from the VECs, EMCMs, OBSs and PTs were interpolated to the same time vector as that of the CCP for direct comparison/utilization between time series.

Pressure transducer data were corrected for atmospheric pressure and converted to water depth using gains and offsets determined by *a priori* laboratory calibrations. The EMCMs and VECs were calibrated by their manufacturers and are highly stable. CCP data were converted to sediment concentration using Archie's Law (Archie, 1942) and the clear-water and packed bed conductivities (Lanckriet *et al.*, 2013). OBS data were calibrated in the laboratory by adding known sediment masses in incremental amounts to a recirculation chamber with a known volume of fluid using sediment samples collected from the bed below the sensor during the study. This aspect of data calibration is the most challenging due to difficulties in maintaining a homogeneous mixture of high sediment concentration of coarse grains. Calibrations were only conducted for concentrations up to 80-100 kg $m^{-3}$. Concentrations beyond this range are reported in this paper assuming the linear relationship can be extrapolated.

The bed level varies throughout each test and during active forcing. Water depths from the PT are adjusted to account for the pre- and post-swash bed level when the area above the PT is known to have zero water depth. Other sensor data must also be adjusted so that they are referenced to a common local vertical datum. The local vertical datum used here is the top of the non-moving sediment bed (bottom of the sheet layer). Vertical distances from this elevation datum are defined on the *z*-axis. Lanckriet *et al.* (2013) defined the sheet layer bottom for CCP data as the elevation where the volumetric concentration is at a loose packing limit of 0.51 (= 1352 kg $m^{-3}$) (Bagnold, 1966a). Alternatively, it is noted that the bed level can also be determined based on the gradient of the instantaneous concentration profile (Lanckriet *et al.*, 2014; O'Donoghue and Wright, 2004). The sharp 'shoulder' transition region in the sheet flow concentration profile is typically co-located with a volume fraction near the loose packing limit. Once the bed level is identified from CCP data, the temporal variability is applied to individual sensor elevations. This means that in addition to each sensor having a time series of its particular measurement it also has an associated time series of elevation relative to the time dependent bed level. Not accounting for this bed level variation can have serious ramifications when estimating bed shear stress as discussed in Puleo *et al.* (2014a) and sediment transport rates for an assumed sensor elevation due to improper elevation for the velocity measurement or incorrect vertical integration limits.

Data for the EMCMs, VECs, CCPs and OBSs were removed from the record when their respective elevation was above the time-dependent free surface. Additional quality control steps are required for VEC data. VEC data were removed when the beam correlation was less than 70 % or the beam amplitudes of at least 2 beams were less than -30 dB (similar to the approach used by Puleo *et al.*, 2012 with these sensors). Poor correlation and weak amplitude is usually associated with bubbles or a large sediment load within the sampling volume. Additionally, VEC data were removed if 1) velocity differences of greater than 0.5 m $s^{-1}$ (corresponding to a clearly erroneous measured flow acceleration of 50 m $s^{-2}$) were recorded between subsequent measurements, 2) if any remaining velocity measurements occurred for time segments of less than 10 samples or 3) a bin was located below the instantaneous bed level.

## 4. Sediment Flux, Sediment Transport and Hydrodynamic Forcing Descriptors

Figure 3 shows a schematic of assumed swash-zone velocity and sediment concentration profiles. The horizontal scale on the sediment concentration graph can be thought of as logarithmic to more adequately account for the rapid transition in concentration from the sheet flow layer to the suspension layer. In practice, calculating the sediment flux should be simply the product of the velocity and concentration profiles. No known field or laboratory swash-zone study has been able to accomplish this “simple” calculation because of measurement gaps and variations in sampling volumes. Although the overall data set collected as part of this study is highly resolved, it still suffers partially from data gap issues. For example, suspended sediment concentration was obtained from only 4 vertical elevations. A pragmatic approach is taken and data are extrapolated in space in an effort to “fill in” the gaps to provide an approximation of the sediment transport. Data are not extrapolated in time (see Section 6). The gap in the concentration profile between the lowest OBS and the top of the sheet layer is approximated by assuming an exponential concentration profile. Gaps in the velocity profile between the lowest valid EMCM reading and the highest VEC bin are approximated with a linear interpolation. No velocities in the sheet layer were measured due to signal attenuation attributed to high sediment and bubble concentrations. In fact, to the authors’ knowledge, no swash-zone velocities in the sheet layer under prototype conditions have ever been measured. However, previous laboratory studies have suggested the velocity profile in the granular sheet layer can be approximated using a maximum velocity at the top of the sheet layer and zero velocity at the bottom of the sheet layer (e.g. Pugh and Wilson, 1999; Wang and Yu, 2007) as

$$u(t,z) = u_{\delta_b}(t)\left(\frac{z}{\delta_b(t)}\right)^n \;\; for\;\; 0 < z \,\le\, \delta_b(t), \qquad (1)$$

where $n$ is positive and ranges from 0.5 to 1, $u_{\delta b}(t)$ is the velocity at the top of the sheet layer, $\delta_b(t)$ is the sheet layer thickness and $z$ is the vertical coordinate with $z$ = 0 at the instantaneous bed level. Thus, the origin for the $z$ coordinate is the bottom of the sheet flow layer and that origin necessarily varies as a function of time as the bottom of the sheet flow layer also varies in time. In Eq. (1) $n$ is set to 1, resulting in a linear velocity profile (See Section 6) and the near-bed velocity at 0.005 m above the *top* of the sheet layer is nominally used for $u_{\delta b}(t)$. The velocity from the next highest VEC bin or EMCM is used in instances where no velocity data are available at 0.005 m above the top of the sheet layer. Utilizing $u_{\delta b}(t)$ in this manner allows for an increased number of sediment transport rates to be determined but does mean that the elevation from which the value is extracted may vary slightly over the swash cycle.

Instantaneous cross-shore suspended sediment flux, $q_{susp}(t,z)$, and cross-shore sheet flow sediment flux, $q_{sheet}(t,z)$, are estimated as

$$q_{susp}(t,z) = u(t,z)SSC(t,z) \tag{2}$$

and

$$q_{sheet}(t,z) = u(t,z)SFSC(t,z) \tag{3}$$

where $u(t,z)$ is the constructed cross-shore velocity obtained from the VEC and EMCM array. Eqs. (2) and (3) are only valid within the suspended load and sheet flow layer regions respectively. Instantaneous suspended load transport, $Q_{susp}(t)$, and sheet load transport, $Q_{sheet}(t)$, are obtained by integrating $q_{susp}(t,z)$ and $q_{sheet}(t,z)$ over the vertical as

$$Q_{susp}(t) = \int_{z_{\delta_b}}^{z_{OBS4}} q_{susp}(t,z)dz \tag{4}$$

and

$$Q_{sheet}(t) = \int_{z=0}^{z_{\delta b}} q_{sheet}(t,z)dz \quad (5)$$

where $z_{\delta b}$ is the elevation of the top of the sheet layer defined to occur where the volumetric concentration is 0.08 (Bagnold, 1966a), $z_{OBS4}$ is the elevation of the highest OBS and $z = 0$ is the instantaneous bed level as defined previously. The integrals are calculated as summations in practice because the velocity and sediment concentration profiles are not known analytically. Combining the two transport rates provides a highly-resolved sediment transport profile from within the sheet layer to ~ 0.08 m above the bed. For clarity, we refer to $q$ as sediment flux and $Q$ as sediment transport throughout the paper.

Sediment transport estimates are generally derived from bed shear stress measurements. The bed shear stress, $\tau$, is estimated from the VEC velocity profile in order to examine potential sediment transport relationships in this study. The mean velocity profile in a fully developed turbulent boundary layer is often quantified using the von Karman-Prandtl relationship

$$u(t,z) = \frac{u_{*(t)}}{\kappa} ln\left(\frac{z}{z_0}\right) \;\; for\; z_{\delta_b} \leq z \leq z_{bl}\,, \quad (6)$$

where $u_*(t)$ is the friction velocity, $\kappa$ (= 0.4) is the von Karman constant and $z_0$ is the roughness height. Eq. (6) is assumed to be valid for mobile beds from just above the top of the sheet layer through to the top of the boundary layer at $z_{bl}$. The relationship is undefined at $z = 0$ so application can only occur for $z > z_0$. Eq. (6) was not originally developed for accelerating or under-developed turbulent boundary layers, but has been used with success under these conditions in past studies (Jensen *et al.*, 1989; O'Donoghue *et al.*, 2010; Puleo *et al.*, 2012). The bed shear stress is related to the friction velocity by

$$\tau\ (t) = \rho u_*(t)|u_*(t)|, \tag{7}$$

where $\rho$ is the fluid density, and | | indicates magnitude in order to maintain the direction of cross-shore shear stress.

The logarithmic model is used to determine $u_*$ for each velocity profile and hence the bed shear stress. A least squares regression between the velocity profile and $ln(z)$ is performed on the VEC profile. Only the lower 0.03 m of the water column is used to estimate the shear stress due to the potential for non-logarithmic profile variability away from the bed. The slope, $s$, of the least squares regression yields $u_* = s\kappa$ and the shear stress is obtained using Eq. (7). The logarithmic model fit, quantified by the square of the correlation coefficient $r^2$, is rejected when it poorly fits the data, as past studies using ensemble-averaged data used an $r^2$ cutoff of 0.9 or more (e.g. O'Donoghue *et al.*, 2010). Data under prototype conditions with fewer "identical" realizations for ensemble-averaging have more variability. An $r^2$ value of 0.7 is used in this study as an indicator of poor model fit to instantaneous data.

## 5. Results

### 5.1 Hydrodynamics and Sediment Concentration

Figure 4 shows hydrodynamic and sediment concentration data from test A2. The water depth exceeds 0.1 m for each event as identified in Figure 4A. Cross-shore velocities from the EMCMs occur within the time frame for each swash event but have a shorter duration due to their elevation. The EMCM higher above the bed (black curve in Figure 4B) only registers a velocity during the deepest parts of the swash cycle. Maximum uprush velocities approach 1.5 m $s^{-1}$ for this test. Measured backwash velocity magnitudes do not exceed 1 m $s^{-1}$ for this test because the water thins rapidly under these forcing conditions leaving the sensor exposed. Suspended sediment concentration peaks near the beginning of the measured portion of the swash cycle (Figure 4C) where velocity data are not fully resolved. Maximum suspended sediment concentrations are generally less than ~100 kg $m^{-3}$ for this test. Corresponding sheet flow concentrations are shown in Figure 4D. Note the difference in the vertical scale and the concentration scale where maximum SFSC exceeds 1300 kg $m^{-3}$. The black curve is the bottom of the sheet flow layer The magenta curve is the top of the sheet flow layer defined at a volumetric concentration of 0.08 (Bagnold, 1956). When the sensor location is inundated there is a rapid decrease in SFSC as material is mobilized landward and carried into the water column leading to the corresponding increase in SSC. SFSC data show increased signal saturation through this roughly 90 s data segment. Signal saturation is indicative of individual profiling points located in the stationary bed and here suggest the bed level increased by ~0.025 m. The same types of signals are seen for test A4 (Figure 5) where the forcing conditions were the same but the lagoon level was lower and the profile was slightly steeper. Cross-shore velocities are quantified throughout more of the backwash due to the EMCMs being closer to the bed at the beginning of the test. Test A6 (Figure 6) displays larger signals than test A2 or A4. The wave period increased from 8 to 12.2 s and the foreshore slope was steeper for Test A6 as compared to the other tests. Water depths at the measurement location (Figure 6A) are more than double those for the other test cases. Maximum velocities (Figure 6B) are similar to the other cases, but both EMCMs record for nearly the same amount of time due to the deeper conditions. Maximum SSC values, unlike those in the other tests, exceed 200 kg $m^{-3}$ and show sharp increases with the swash arrival. SSC peaks are also occasionally observed in the backwash. SFSC trends show a fairly stable time-averaged bed level (Figure 6D). The beach profile at the beginning of the test was steeper than in test A2 and A4 and perhaps in quasi-equilibrium causing the bed to change little in a mean sense. During an individual swash inundation, though, the bed level dropped rapidly by ~ 0.02 m. Sediment is deposited near and during flow reversal as indicated by an increase in SFSC during these times. Sediment is again mobilized in the sheet layer during backwash but not to the same depth as that for uprush.

Only EMCM velocities were shown in Figures 4-6. VEC velocities provide an indication of the vertical variability as a function of time. Figure 7 shows an example of 3 swash events from test A2. Cross-shore velocity time series from several elevations above the top of the sheet layer are similar to those from the EMCM (Figure 7A; gray and black curves). EMCM velocities are difficult to see in the figure due to their consistency (magnitude and phasing) with the VEC velocities. Vertical profiles of the cross-shore velocity (Figure 7B) are extracted from the record at the times identified by the vertical dotted (uprush) and solid (backwash) lines in Figure 7A. Uprush (backwash) velocities are indicated by open (closed) circles. The boundary layer is thicker at the beginning of the swash cycle and appears to show a thinning until near flow reversal (Figure 7B; the “kink” in the velocity profile near an elevation of 0.03 m for the red circles progressively decreases to about 0.02 m for the cyan to black to magenta open circles).

There is no boundary layer at flow reversal (Figure 7B; filled red circles). Boundary layer formation happens rapidly and is seen to grow throughout the backwash (Figure 7B, cyan to blue to magenta to black filled circles) until the sensor emerges from the water column.

5.2 Sheet Flow and Suspended Sediment Fluxes

Example sheet flow and suspended sediment fluxes for test A2 are shown in Figure 8. Water depths (Figure 8A) are shown for context and event beginning and end times. Suspended sediment fluxes at 4 different elevations indicate considerable differences in magnitudes with distance away from the bed (Figure 8B). Maximum suspended sediment flux magnitudes exceed 100 kg $m^{-2}$ $s^{-1}$ during uprush and backwash. Sheet flow sediment flux is also shown at several elevations above the bed (Figure 8C). Sheet flow sediment flux magnitudes are larger than those for suspended sediment fluxes (note the difference in the vertical axis range between Figures 8B and 8C). Uprush sheet flow flux magnitudes exceed 300 kg $m^{-2}$ $s^{-1}$ while those in the backwash exceed 500 kg $m^{-2}$ $s^{-1}$ for the few events shown here. Vertical variability of the sediment fluxes (Figures 8D,E) is shown for ten time instances depicted by the vertical lines in Figure 8C. Dotted vertical lines and corresponding flux profiles are for uprush while solid lines and corresponding flux profiles are for backwash. Suspended sediment flux profiles (Figure 8D) show decreased values as the bed is approached but do not reach zero since the flow velocity for suspended load does not reach exactly zero at the top of the sheet layer. Flux profiles near flow reversal are more varied and do not show as much indication of a boundary layer as expected. Suspended sediment flux profiles extend to a maximum of about 0.07 m above the bed. The assumption of a linear velocity profile had to be invoked for the lower part of the water column and near the uprush initiation due to poor velocity quantification (see for instance the red dotted and black dotted lines in Figure 8D). Corresponding sheet flow sediment flux profiles are suggestive of a boundary layer like transition through the sheet flow layer (Figure 8E). However, the profile shape results more from the shape of the sediment concentration profile than the assumed linear velocity profile through the sheet layer. Sheet flow flux profiles can extend to about 0.02 m above the bed during uprush but are more typically confined to about 0.01 m above the bed for the rest of the swash duration. Sheet flow flux profile magnitudes for backwash generally exceed corresponding profiles for uprush as expected from Figures 8B,C (note the difference in the horizontal scales between Figures 8D,E).

Sediment flux profiles from Figure 8 are integrated over depth using Eqs. (4,5) to quantify the suspended load and sheet load transport (Figure 9). Water depths are shown in Figure 9A for temporal context. Suspended load transport magnitudes (black curves in Figure 9B) approach 5 kg $m^{-1}$ $s^{-1}$ during uprush but are generally less during the recorded portion of the backwash. Sheet load transport magnitudes (grey curves in Figure 9B) are similar for both uprush and backwash with maximum magnitudes exceeding 2 kg $m^{-1}$ $s^{-1}$. The time series indicate that suspended load transport exceeds that of sheet load transport during uprush and is similar in magnitude during backwash. The ratio between the two sediment load transport magnitudes is defined as

$$Q_{ratio} = \begin{cases} Q_{susp}/Q_{sheet} & when\ Q_{susp} \geq Q_{sheet} \\ Q_{sheet}/Q_{susp} & when\ Q_{susp} < Q_{sheet} \end{cases} \qquad (8)$$

$Q_{ratio}$ is shown in Figure 9C where black dots indicate a dominance of suspended load transport and grey dots a dominance of sheet load transport. A $Q_{ratio}$ value of 1, identified by the horizontal dotted line indicates the sediment load transport magnitudes are equal. The transport ratio approaches 8 during uprush and is generally confined to near 1 during backwash. The mean ± standard deviation for instantaneous suspended load transport dominance is 4.48±5.90 while that for instantaneous sheet load dominance is 6.03 ± 26.4. The interquartile range (IQR) is 1.55-4.70 and 1.13-1.88 for suspended load and sheet load dominated portions of the swash zone, respectively. The IQR is meant to give another indication of the spread in the transport estimates. Figure 9C indicates that much of the suspended load dominance occurs during uprush while sheet load dominance occurs during backwash. The main reason suspended load transport is a significant contribution to uprush transport is that sheet flow layer is generally only ~0.01 m thick whereas the suspended load layer used in the calculations is often over 0.06 m thick  Thus, even though the instantaneous flux estimates for sheet flow often exceed those for suspended sediment flux by a factor of 2 or more, the restricted range over which the transport mode occurs reduces its overall influence on the total load transport rate during uprush.

### 5.3 Ensemble-Averaged Transport Estimates

Figure 9 showed the transport rate estimates for test A2 only and for just a few swash events. Ensemble-averaging is undertaken to show similar results for a typical swash event and for the different test cases (Figure 10). Swash events are defined during each test case based on the water depth time series that goes to zero in between individual swash events. Velocities and sediment concentrations are interpolated to a time vector at 8 Hz with a duration corresponding to the wave period (Table 1). Averaging is only carried out across the space and time positions when data exist so that the average is not artificially skewed by missing data. Only several waves are used for each average in an effort to compile events that are similar. That is, waves are only considered when the bed is identifiable for the majority of the cycle and sheet flow exists within the measurement range of the sensor. Thus, several waves are often removed from the beginning and end of the test case (e.g. first few waves in Figure 5; test A4 are not used). Six waves are used for ensemble-averaging for test A2, 8 for test A4 and 12 for test A6. This method provides statistically robust estimates, but is biased towards the lower forcing conditions when there is less morphologic change. Suspended sediment flux profiles are shown as a colormap for the three tests (Figure 10A-C). Note the difference in the color scale for test A6. Ensemble-averaged suspended sediment flux profile values are largest during uprush and exceed 50 kg $m^{-2}$ $s^{-1}$ for test A2, 20 kg $m^{-2}$ $s^{-1}$ for test A4 and 180 kg $m^{-2}$ $s^{-1}$ for test A6 (Figure 10A-C). Ensemble-averaged uprush sheet flow flux profile values exceed 200 kg $m^{-2}$ $s^{-1}$ in all cases but are largest for test A6 (Figure 10D-F). Sediment load transport magnitudes vary considerably for the three test cases (Figure 10G-I). The weakest transport magnitudes are found for test A4 even though the forcing and foreshore slope conditions are similar to test A2. A possible explanation is the higher lagoon level during test A2 that may increase bed saturation enhancing sediment mobility. The largest transport magnitudes are found for test A6 with a wave height similar to test A2 and A4 but with a longer period and a steeper foreshore. In all cases the suspended load transport exceeds the sheet load transport during uprush (Figure 10J-L; Table 2). Sheet load transport is similar to suspended load transport during backwash for test cases A2 and A4. Sheet load transport dominates during backwash for test A6 (Table 2).

## 5.4 Shear Stress and Sediment Transport Prediction

Bed shear stresses are estimated for the ensemble average event using eq. (7) and the approach described in Section 4 (Figure 11). Shear stress magnitudes are largest during backwash and exceed 40 N $m^{-2}$ for all three test cases. There is no clear dominance of one test case over another with regard to bed shear stress during backwash. Estimated uprush bed shear stresses tend to be smaller than those in the backwash except for test A2. This result is counter to general expectations on a steep natural beach and recent laboratory findings (e.g. Kikkert *et al.*, 2013). Differences in bed shear stress magnitudes between uprush and backwash are likely to stem from the lack of data during the initial phases of uprush when the sensor just becomes immersed and the flow contains a large void fraction.

Sediment transport in coastal environments is often related to some type of an energetics formulation (e.g. Bagnold, 1966b; Bailard, 1981). The main components of the energetics formulation are a mobilizing term, the bed shear stress, and a transport agent: the velocity. In its most simplistic form the model can be written as

$$Q_s(t) = k\frac{1}{g}\tau(t)u(t)\ , \qquad (9)$$

where $Q_s$ is the sediment transport rate, $g$ is gravitational acceleration (= 9.81 m $s^{-2}$) and $k$ is a dimensionless constant. The velocity $u$ has to be obtained from some elevation. Here, the velocity from the top of the measured cross-shore velocity profile from the Vectrino II is used. The formulation for nearbed and suspended load transport in their most basic forms are similar so that eq. (9) can be used for either transport mode (or the total transport) by varying $k$. The transport potential defined as eq. (9) with the *k* set to unity is shown in Figure 11B. The transport potential is weak during uprush except for test A2 and exceeds 2 kg $m^{-1}$ $s^{-1}$ during backwash for the three test cases. Figures 11C,D show the model estimated transport (horizontal axis) in relation to the transport estimates from the in situ ensemble-averaged measurements (vertical axis). Comparisons are made for suspended load (Figure 11C) and sheet load (Figure 11D) separately. Linear fits are carried out for uprush and backwash individually and the correspondence between the model estimate and estimate from in situ data are fairly linear (Table 3) with slope values, *k*, ranging from 0.24 to 24.7 for suspended load transport and 0.28 to 6.2 for sheet load transport. Uprush *k* values exceed corresponding backwash *k* values for the 3 tests and both transport types. The largest values for *k* occur for test A6. The majority of the other *k* values are less than 1 but still show considerable spread.

## 6. Discussion

Data in this study are some of the most complete prototype swash-zone sediment transport and velocity measurements ever collected and are used to determine the importance of suspended sediment to sheet flow sediment transport. It is found that generally the depth-integrated suspended load is dominant during uprush while depth-integrated sheet load is comparable to depth-integrated suspended load during much of the backwash. These findings are in general agreement with those of past work suggesting the uprush is probably dominated by suspended load transport (Masselink *et al.*, 2005; Puleo *et al.*, 2000). The results are also consistent with previous findings associated with swash-zone sheet flow measurements (Lanckriet *et al.*, 2014; Puleo *et al.*, 2014b). Backwash suspended and sheet load transport was 6-8 kg $m^{-1}$ $s^{-1}$ (compared to up to ~7 kg $m^{-1}$ $s^{-1}$ for this study) under more prolonged backwash. Maximum uprush suspended load transport exceeded maximum uprush sheet flow transport in the Puleo *et al.* (2014b) study by approximately a factor of 2 and is also consistent with the findings in the present study for Test A2 and A6. It is noted, however, that the analysis in Puleo *et al.* (2014b) study was not performed to the same level of detail as here regarding the velocity and concentration data as a function of space and time. The effect of spatial and temporal data gaps and variations on the estimated transport rates depending on assumptions made in the calculations in the present study are discussed further.

## 6.1 Spatial Data Gaps

A major difficulty in determining the importance of one transport mode over another is measuring the entire velocity and sediment flux profile. We were not able to fully overcome this challenge even though the data have bridged a significant gap by including sheet flow estimates. The measurements in this study required spatial interpolation near uprush initiation when velocity measurements tend to be difficult to capture reliably, throughout other portions of the swash cycle when acoustic data reliability indicators were poor and simply because the EMCMs were located some distance above the VECs. Another potential effect of spatial data gaps is the inability for the sheet flow layer flux profiles to merge smoothly with the suspended sediment flux profiles at the top of the sheet layer (see for example the horizontal offsets between corresponding curves in Figure 8D,E). However, other researchers (Dohmen-Janssen and Hanes, 2005; their Figure 13) have also shown the difficulty in aligning flux estimates from the two transport regions.

## 6.2 Temporal Data Gaps

Spatial data gaps are compounded by temporal data gaps. Simple statistics involved in time averaging when data gaps are biased toward particular wave phases would suggest that the temporal data gaps are of more concern when quantifying swash-zone sediment transport. It is evident from Figures 8-11 that much of the velocity and transport signals from the swash zone are artificially truncated. The time axis in all figures are true to the swash event duration based on water depth but more than half of the event duration has no velocity or sediment flux data record. Sensor data are usually noisy when first immersed during uprush initiation causing the initial stages to be missed. Lack of data is also a major concern during backwash. Velocity sensor emergence from the water column during the thinning backwash renders a substantial portion of the event un-measured in terms of sediment transport (the CCP can still measure the sheet flow concentration but has no corresponding velocity that enables calculation of flux). Note, that data gaps in either phase of the swash cycle have the potential to alter the calibration coefficients when correlating “measured” to predicted sediment transport rates.

As alluded to earlier, temporal gaps in the time series cannot be overcome with an in situ velocity sensor that must be located some elevation above the at-rest bed. Remote sensing is one approach that may overcome this issue. An example is the use of particle image velocimetry from a downward-looking imager to quantify the surface velocity as the flow thins (Lawless, 2013). The technique cannot predict velocities below the surface but a surficial velocity throughout the duration of the event would enhance the ability to estimate sediment transport rates. No effort was undertaken in this study to extend the measurements temporally because the velocity time history shape is difficult to determine *a priori*. Puleo *et al.* (2014b) discussed and Lawless (2013) showed that the velocity in the backwash can slow considerably as the water depth thins and friction begins to dominate gravitational forces. Having knowledge of the velocity and sediment transport rates throughout the entire swash duration could lead to different results than those obtained here. We speculate that the major difference would be a larger dominance of sheet flow transport during backwash as the flow thins (Figure 12) and there is less vertical capacity for suspended load transport. Swash zone water depths during the test cases shown here and indeed on most intermediate to reflective beaches exhibit a depth time series similar to that shown in Figure 12A. The velocity from a current meter can only be measured for the duration contained by the two vertical dotted lines. A short portion of the velocity record during uprush is lost due to depth and sensor disturbance issues (Figure 12B). A much longer portion of the velocity record is lost during backwash due to the shallow depths. The lack of data during this time makes identifying the overall importance of sheet flow sediment transport difficult. Figure 10I showed an increase in the $Q_{ratio}$ during backwash when sheet flow dominates but the ratio decreases at the end of the measurement portion. The decrease is likely due to weaker velocity measurements as the current meter begins to emerge. But as the depth continues to decrease, the importance of sheet flow transport may increase even though the velocity is expected to decrease (Figure 12C). At some time during backwash flow the depth will reach a point where there may be sheet flow transport only. Comparing sheet flow to suspended sediment transport during these instances is not possible, and indeed transport during these instances has yet to be measured but visible observation suggests the transport during this time is still significant.

### 6.3 Sediment Transport

Energetics sediment transport formulations have been used in the swash zone for many studies (e.g. Butt *et al.*, 2005; Hughes *et al.*, 1997; Masselink *et al.*, 2005; Puleo *et al.*, 2000). The general consensus is that the simple formulations are not adequate for predicting swash zone sediment transport. Model modifications have been made in an effort to enhance the predictive capability (Butt *et al.*, 2001; Butt *et al.*, 2004; Puleo *et al.*, 2003b) but the predictive skill was still limited. The results shown here are somewhat similar to past studies but indicate there is only moderate at best model skill using the simple approach. This is evident from the wide range of $k$ values (Table 3). Many past field efforts used a coarse representation of the velocity and/or sediment concentration profile and none had detailed measurements of the sheet load transport. Those coarse measurements may be somewhat responsible for the poor to moderate predictive skill of the energetics approach when applied to swash-zone field data. It is not clear if this is the case here because even the level of detail in this study is not adequate to fully indicate model skill throughout an entire swash event.

## 6.4 Sensitivity of Transport Estimates

Sediment transport results were presented using ensemble averaging approaches and through depth integration. While each event used in a particular ensemble average is similar, they are not identical. Variability is presented for the sediment transport rates (Figure 13) as that is the most straightforward for graphical presentation and generally the quantity of interest with respect to sediment transport studies. The range provided as the depth-integrated ensemble average ± the standard deviation is roughly the same for sheet flow and suspended sediment transport (Figure 13A,D,G) except during the largest uprush transport. There, the suspended load transport estimate can vary up to almost 50 % for some tests. Sediment transport in the sheet flow layer had less variability except for test A4 (Figure 13D) during the backwash.

The variability presented relies solely on the ensemble averaging assuming the individual measurements are without error. There are numerous factors that can introduce errors into the measurements including the sensors themselves. Variability in the sheet flow thickness would alter the region over which that transport type is calculated. However, the original work with the CCP sensor showed the sheet flow thickness estimates using either the shape of the concentration profile (Lanckriet *et al.*, 2014; O'Donoghue and Wright, 2004) or a concentration cutoff indicative of a loose packed bed (Bagnold, 1966a) are similar. Optical backscatter sensors also have the potential for introducing error. OBS calibration can be problematic especially for coarse grains that are difficult to suspend homogeneously. Calibrations are performed using sediment collected from the bed below the sensor (unless pump samples are taken). However, the distribution of the material in suspension during data collection versus that composing the bed material is almost certainly different. These differences will manifest in the calibration in an unknown manner. Bubbles have also been shown to artificially increase the OBS measurement by up to 25 % (Puleo *et al.*, 2006). If the OBS values during uprush were in error by that percentage then the difference between the estimated suspended and sheet flow sediment transport rates would decrease but not enough for sheet flow transport to become dominant in tests A2 and A6 (i.e. multiply the suspended load transport rates in Figure 13A,D,G by 0.75).

The method used to estimate sediment transport can also induce error in the calculation. Sheet load transport was estimated assuming a linear extrapolation of the velocity profile through the sheet layer. Previous studies have shown that the velocity profile may vary with an exponent of 0.5 or 0.75 (Sumer *et al.*, 1996; Wang and Yu, 2007). Sheet load transport increases in general and for some portions of the cycle by over 60 % when the velocity profile in the sheet flow layer is recalculated using an exponent of 0.5 (Figure 13B,E,H). The range on the sheet load transport estimates also increases.

No effort was undertaken originally to extend the velocity or suspended sediment transport profile to the free surface. There are a variety of options for doing such a calculation (all potentially introducing additional unknown error): a) assume the flow and concentration are vertically uniform above the highest submerged OBS, b) linearly extrapolate the concentration above the highest submerged OBS using the sediment concentration gradient from the two highest submerged OBS, c) linearly extrapolate the sediment concentration from the highest submerged OBS to zero at the free surface or d) try to fit the concentration and velocity profiles to some theoretical formulation and extend those profiles to the free surface, among many other options. The depths in the swash zone during this study rarely exceeded 0.2 m and the velocity profiles (Figure 7) become more uniform above the lower 0.05 m of the water column so the assumption of uniform velocity above the highest submerged OBS is adopted. Sediment concentrations above the highest submerged OBS are estimated using a hybrid approach. The concentration gradient is used for extrapolation. However, if the concentration at the free surface would become negative or larger than the concentration at the highest submerged OBS it is forced to 0 kg $m^{-3}$. The latter case could occur if, for example, the concentration was larger at OBS 4 than at OBS 3 causing an increasing concentration with elevation.

Extending the transport estimates to the free surface using any approach will enhance the importance of suspended load transport, mostly during uprush due to increased water depths. The additional calculations described confirm this supposition (Figure 13C,F,I). Increases in suspended sediment transport are most evident for tests A2 and A6 with the maximum sediment transport rate increasing by up to ~110 % for test A6 (Figure 13I). It is noted that the maximum water depths during test A6 were nearly double the maximum water depths for the other two cases and that is a primary factor in the large change in the sediment transport rate estimate.

## 7. Conclusion

A large-scale laboratory experiment was conducted on a coarse sand beach to determine the relative importance of sheet flow compared to suspended sediment transport. Despite challenges in the spatial and temporal sampling, the observations provide strong evidence for the following findings.

1) Sheet flow sediment flux profiles are generally larger in maximum magnitude than the corresponding suspended sediment flux profiles regardless of swash phase.
2) Depth integration of the flux profiles indicate that suspended sediment transport dominates during uprush whereas sheet load transport is of similar magnitude during backwash for the 8 s waves with a 1:8.7 slope and dominates during backwash for the 12.2 s waves with a 1:6.5 slope.
3) The limited vertical range over which the sheet load transport occurs relative to the suspended load transport is a controlling factor in determining which transport mode dominates.
4) Even for “highly” resolved data, spatial interpolation is required to fill in data gaps when velocity profiles are noisy.
5) Temporal data gaps are a major limitation in quantifying the importance of the transport modes through an entire swash event where much of the backwash is artificially truncated due

to lack of velocity measurements from an elevated current meter. These data gaps must be circumvented using remote sensing or other miniature sensors in future swash zone experiments.

6) Additional calculations were undertaken in an effort to account for the sediment transport that was missing due to data gaps or due to estimates of the sheet flow velocity profiles. The general findings are not altered except that the uprush dominance by suspended load increases if sediment transport is extrapolated to the free surface and sheet flow becomes more important if the velocity profile extending into the sheet layer decays as a quadratic function rather than linear.

## Acknowledgements

The work described in this publication was supported by the European Community's 7th Framework Programme through the grant to the budget of the Integrating Activity HYDRALAB IV, contract no. 261520. Additional funding for JAP was provided by the University of Delaware, the National Science Foundation (grant no. OCE-0845004 and OCE- 1332703) and the US/UK Fulbright Commission. TL was supported by the National Science Foundation (grant no. OCE-0845004). DF was partially supported by the National Science Foundation.This work was also partially supported by the Engineering and Physical Sciences Research Council of the UK (grant no. EP/K000306/1). We thank the Delta Flume staff for their technical expertise and assistance and the numerous collaborating researchers for their participation. Two anonymous reviewers provided detailed and critical reviews of this work. Additional calculations related to sensitivity were suggested by both.

## References

Alsina, J. M., and Caceres, I. 2011, Sediment suspension events in the inner surf and swash zone. Measurements in large-scale and high-energy wave conditions, Coastal Engineering, 58, 657-670.

Archie, G. 1942, The electrical resistivity log as an aid in determining some reservoir characteristics, Institute of Mining and Metallurgical Transactions, 14, 54-62.

Bagnold, R. A. 1956, The flow of cohesionless grains in fluids, Proceedings of the Royal Society of London, 249(964), 235-297.

Bagnold, R. A. 1966a, The shearing and dilatation of dry sand and the’singing’mechanism., Philosophical Transactions of the Royal Society of London. Series A, Mathematical and Physical Sciences,, 295(1442), 219-232.

Bagnold, R. A. 1966b, An approach to the sediment transport problem from general physics, *422-I*, 37 pp, U.S. Geological Survey, Washington, DC.

Bailard, J. A. 1981, An energetics total load sediment transport model for a plane sloping beach, Journal of Geophysical Research, 86(C11), 938-954.

Blenkinsopp, C., Mole, M. E., Turner, I. L., and Peirson, W. L. 2010, Measurements of the time-varying profile across the swash zone using an industrial LIDAR, Coastal Engineering, 57, 1059-1065.

Blenkinsopp, C. E., Turner, I. L., Masselink, G., and Russell, P. E. 2011, Swash zone sediment fluxes – field observations, Coastal Engineering, 58, 28-44.

Butt, T., and Russell, P. 1999, Suspended sediment transport mechanisms in high-energy swash, Marine Geology, 161(2-4), 361-375.

Butt, T., Russell, P., and Turner, I. 2001, The influence of swash infiltration-exfiltration on beach face sediment transport:  onshore or offshore?, Coastal Engineering, 42(1), 35-52.

Butt, T., Russell, P., Puleo, J. A., and Masselink, G. 2005, The application of Bagnold-type sediment transport models in the swash zone, Journal of Coastal Research, 21, 887-895.

Butt, T., Russell, P., Puleo, J. A., Miles, J., and Masselink, G. 2004, The influence of bore turbulence on sediment transport in the swash and inner surf zones, Continental Shelf Research, 24, 757-771.

Butt, T., Tinker, J., Masselink, G., O'Hare, T. J., and Russell, P. 2009, Field observations of sediment fluxes in the inner-surf and swash zones, Journal of Coastal Research, 25(4), 991-1001.

Conley, D. C., and Beach, R. A. 2003, Cross-shore sediment transport partitioning in the nearshore during a storm event, Journal of Geophysical Research, 108, 3065.

Craig, R. G. A., Loadman, C., Clement, B., Canada, B. H., Rusello, P. J., and Siegel, E. 2011, Characterization and Testing of a new Bistatic Profiling Acoustic Doppler Velocimeter□: The Vectrino-II, Curr. Waves Turbul. Meas., IEEE/OES 1, 246–252.

Dohmen-Janssen, M., and Hanes, D. M. 2005, Sheetflow and suspended sediment due to wave groups in a large wave flume, Continental Shelf Research, 25, 333-347.

Holland, K. T., Puleo, J. A., and Kooney, T. 2001, Quantification of swash flows using video-based particle image velocimetry, Coastal Engineering, 44, 65-77.

Horn, D. P., and Mason, T. 1994, Swash zone sediment transport modes, Marine Geology, 120(3-4), 309-325.

Hughes, M. G., Masselink, G., and Brander, R. W. 1997, Flow velocity and sediment transport in the swash zone of a steep beach, Marine Geology, 138(1-2), 91-103.

Jensen, B. L., Sumer, B. M., and Fredsoe, J. 1989, Turbulent oscillatory boundary layers at high Reynolds numbers, Journal of Fluid Mechanics, 206, 265-297.

Kikkert, G. A., Pokrajac, D., O'Donoghue, T., and Steenhauer, K. 2013, Experimental study of bore-driven swash hydrodynamics on permeable rough slopes, Coastal Engineering, 79, 42-56.

Lanckriet, T. M., Puleo, J. A., and Waite, N. 2013, A conductivity concentration profiler for sheet flow sediment transport, IEEE Journal of Oceanic Engineering, 38(1), 55-70.

Lanckriet, T. M., Puleo, J. A., Masselink, G., Turner, I. L., Conley, D. C., Blenkinsopp, C., and Russell, P. 2014, A comprehensive field study of swash-zone processes, Part 2: Sheet flow sediment concentrations during quasi-steady backwash, Journal of Waterway Port Coastal and Ocean Engineering, 140(1), 29-42.

Lawless, P. 2013, Experimental investigations into the use of particle image velocimetry to quantify wave backwash velocities, 122 pp, University of New South Wales, Sydney, Australia.

Li, X., and Meijer, G. C. M. 2005, A low-cost and accurate interface for four-electrode conductivity sensors, IEEE Transactions on Instrumentation and Measurement, 54, 2433-2437.

Masselink, G., Evans, D., Hughes, M. G., and Russell, P. 2005, Suspended sediment transport in the swash zone of a dissipative beach, Marine Geology, 216(3), 169-189.

Masselink, G., Russell, P., Turner, I., and Blenkinsopp, C. 2009, Net sediment transport and morphological change in the swash zone of a high-energy sandy beach from swash event to tidal cycle time scales, Marine Geology, 267, 18-35.

Masselink, G., Ruju, A., Conley, D. C., Turner, I., Ruessink, B. G., Matias, A., Thompson, C., Castelle, B., and Wolters, G. this issue, Large-scale Barrier Dynamics Experiment II

(BARDEX II): experimental design, instrumentation, test programme and data set, Coastal Engineering.

O'Donoghue, T., and Wright, S. 2004, Concentrations in oscillatory sheet flow for well sorted and graded sands, Coastal Engineering, 50, 117-138.

O’Donoghue, T. O., Pokrajac, D., and Hondebrink, L. J. 2010, Laboratory and numerical study of dam-break-generated swash on impermeable slopes, Coastal Engineering, 57(5), 513-530.

Pugh, F. J., and Wilson, K. C. 1999, Velocity and concentration distributions in sheet flow above plane beds, Journal of Hydraulic Engineering, 125, 117-125.

Puleo, J. A. 2009, Tidal variability of swash-zone sediment suspension and transport, Journal of Coastal Research, 25, 937-948.

Puleo, J. A., Lanckriet, T. M., and Wang, P. 2012, Nearbed cross-shore velocity profiles, bed shear stress and friction on the foreshore of a microtidal beach, Coastal Engineering, 68, 6-16.

Puleo, J. A., Lanckriet, T. M., and Blenkinsopp, C. 2014a, Bed level fluctuations in the inner surf and swash zone of a dissipative beach, Marine Geology, 349(1), 99-112.

Puleo, J. A., Beach, R. A., Holman, R. A., and Allen, J. S. 2000, Swash zone sediment suspension and transport and the importance of bore-generated turbulence, Journal of Geophysical Research, 105(C7), 17021-17044.

Puleo, J. A., Farquharson, G., Frasier, S. J., and Holland, K. T. 2003a, Comparison of optical and radar measurements of surf and swash zone velocity fields, Journal of Geophysical Research, 108(C3), 45-41 - 45-12.

Puleo, J. A., Faries, J. W. C., Davidson, M., and Hicks, B. 2010, A conductivity sensor for nearbed sediment concentration profiling, Journal of Oceanic and Atmospheric Technology, 27, 397-408.

Puleo, J. A., Holland, K. T., Plant, N., Slinn, D. N., and Hanes, D. M. 2003b, Fluid acceleration effects on suspended sediment transport in the swash zone, Journal of Geophysical Research, 108, 3350, doi: 10.1029/2003JC001943.

Puleo, J. A., Johnson, R. V., II, Butt, T., Kooney, T., and Holland, K. T. 2006, The effect of bubbles on optical backscatter sensors, Marine Geology, 230, 87-97.

Puleo, J. A., Blenkinsopp, C., Conley, D. C., Masselink, G., Turner, I. L., Russell, P., Buscombe, D., Howe, D., Lanckriet, T. M., McCall, R. T., and Poate, T. 2014b, A comprehensive field study of swash-zone processes, Part 1: Experimental design with examples of hydrodynamic and sediment transport measurements, Journal of Waterway Port Coastal and Ocean Engineering, 140((1)), 14-28.

Raubenheimer, B. 2002, Observations and predictions of fluid velocities in the surf and swash zones, Journal of Geophysical Research, 107(C11, 3190, doi:10.1029/2001JC001264).

Raubenheimer, B., Elgar, S., and Guza, R. T. 2004, Observations of swash zone velocities: A note on friction coefficients, Journal of Geophysical Research, 109, C01027, doi:01010.01029/02003JC001877.

Ruju, A., Conley, D., Austin, M., Puleo, J.A., Lanckriet, T., Foster, D., Masselink, G. this issue, Boundary layer dynamics under large-scale laboratory Conditions, Coastal Engineering.

Sumer, B. M., Kozakiewicz, A., Fredsoe, J., and Deigaard, R. 1996, Velocity and concentration profiles in sheet-flow layer of movable bed, Journal of Hydraulic Engineering, 122(10), 549-558.

Turner, I., Russell, P., and Butt, T. 2008, Measurement of wave-by-wave bed-levels in the swash zone, Coastal Engineering, 55, 1237-1242.

Wang, Y. H., and Yu, G. H. 2007, Velocity and concentration profiles of particle movement in sheet flows, Advances in Water Resources, 30, 1355-1359.

Wengrove, M. E., and Foster, D. L. 2014, Field evidence of the viscous sublayer in a tidally forced developing boundary layer, Geophysical Research Letters, 41,, 5084–5090.

Yu, Z., Niemeyer, H. D., and Bakker, W. T. 1990, Site investigation on sand concentration in the sheet flow layer, ASCE, New York, 2360-2371 pp.

Figure Captions

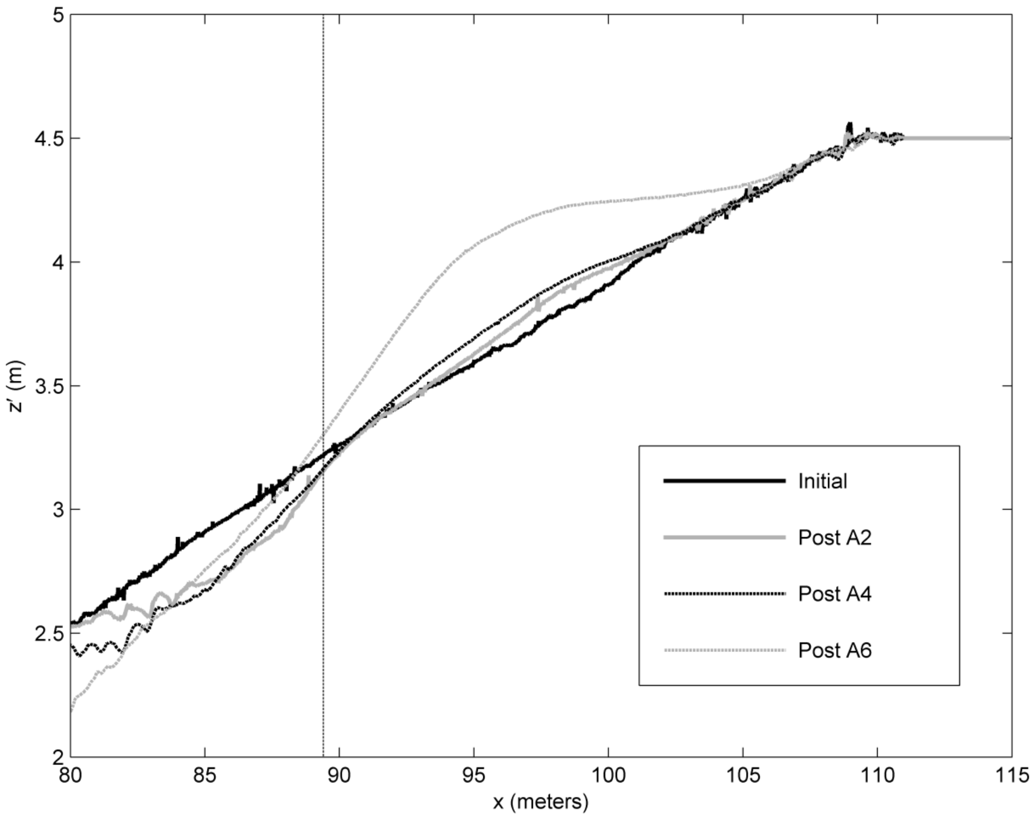


Figure 1. The initial planar beach profile and those collected following each monochromatic test case. The vertical dotted line indicates the cross-shore location of the sensors used in this paper.


Figure 2. A) Photo showing sensors used in this paper. Two Vectrino II profiling velocimeters (VECs; 1), two conductivity concentration profilers (CCPs; not visible) below the VECs, two Valeport electromagnetic current meters (EMCMs; 2), one Druck pressure transducer (PT) buried below the EMCMs, four Campbell Scientific optical backscatter sensors (OBS; 3). B)

Photo of the CCP showing the measurement section and the electronics housing. C) Close-up photo of the region denoted by the black box in A. Photo shows one of the CCPs deployed with only the measuring section exposed to the flow.

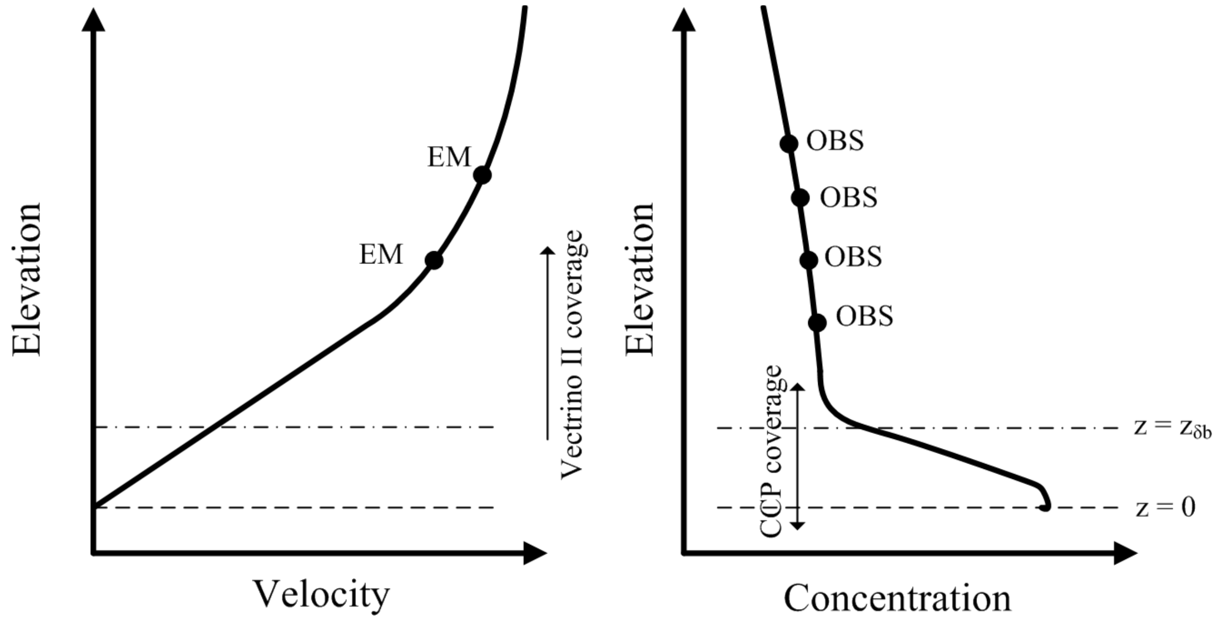


Figure 3. Schematic showing velocity and sediment concentration profiles in the lower portion of the water column and the expected sensor coverage.

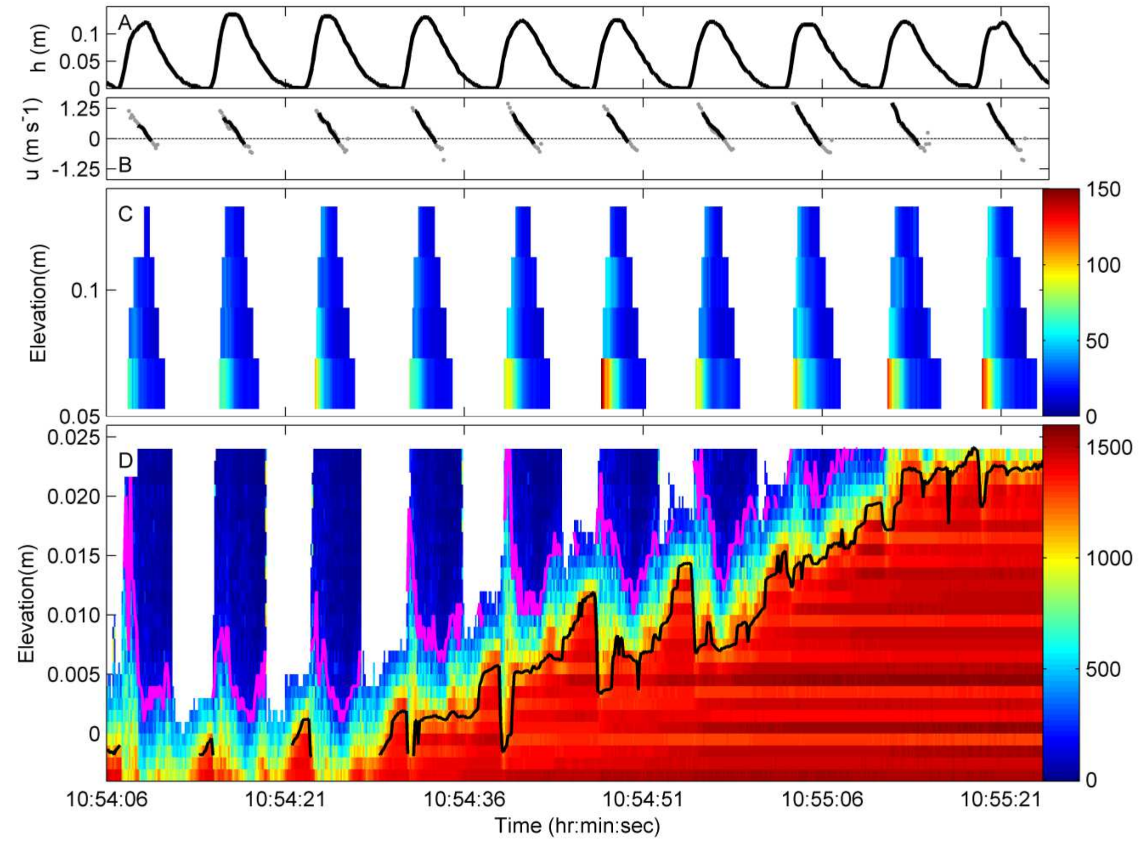


Figure 4. Example data from test A2. A) Water depth. B) Cross-shore velocity from the 2 EMCMs. Black dots indicate the sensor higher in the water column and gray dots indicate the sensor lower in the water column. C) OBS data from the 4 sensors. D) CCP data in the active sheet layer. The color scale for C and D is in kg $m^{-3}$ and the elevation is relative to the bed level at the beginning of the run. The black and magenta curves identify the bottom and top of the

sheet flow layer respectively.

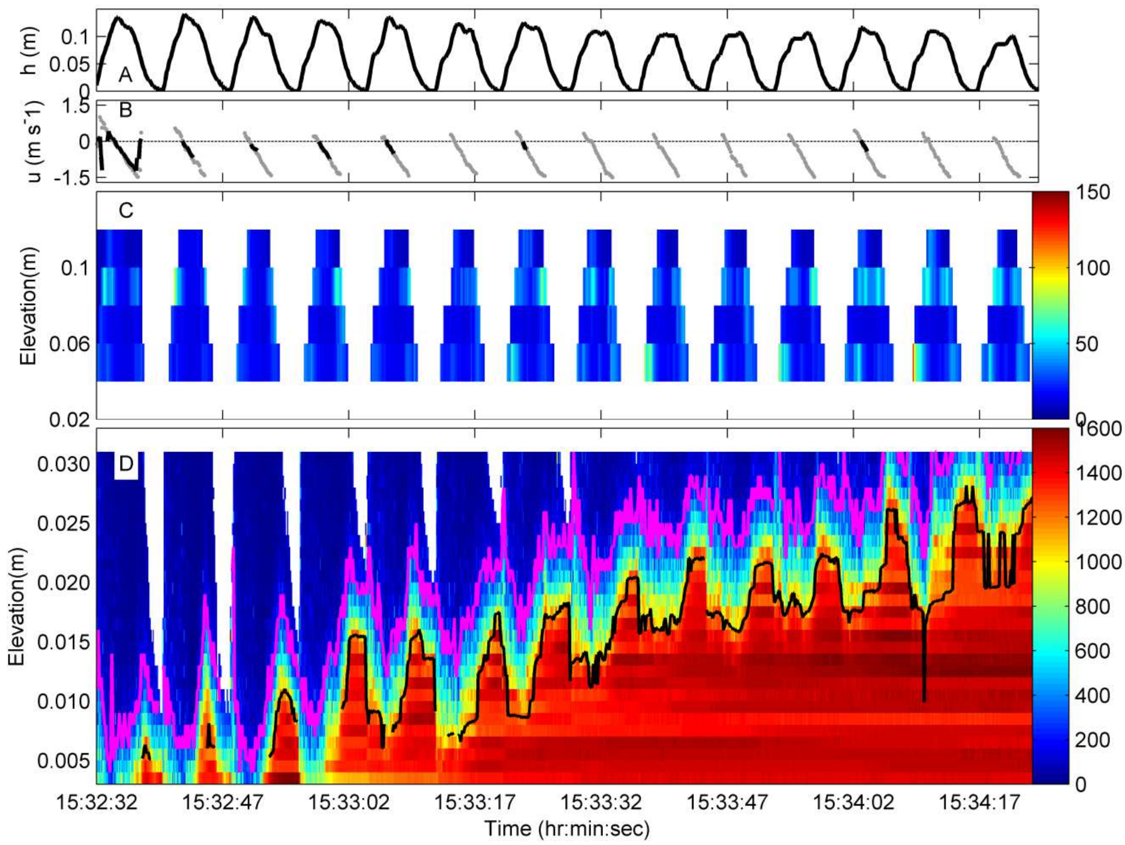


Figure 5. Example data from test A4. Description as per Figure 4.

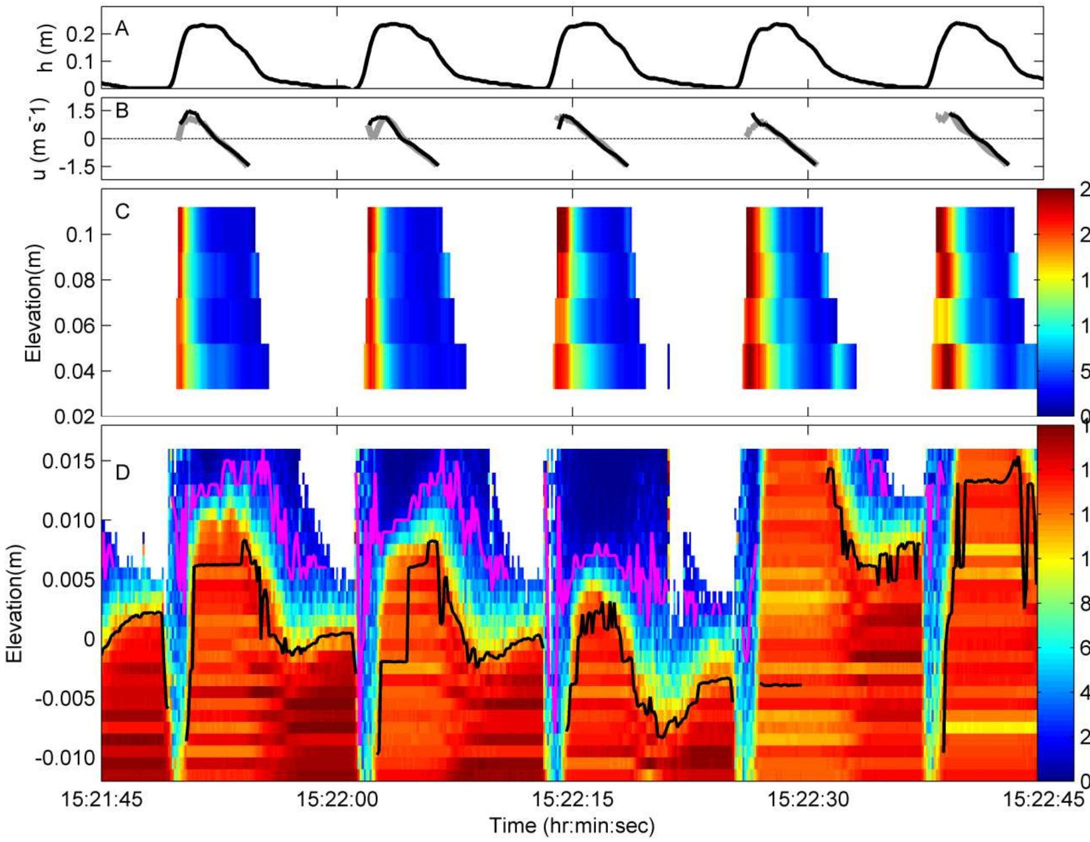


855

856 Figure 6. Example data from test A6. Description as per Figure 4.

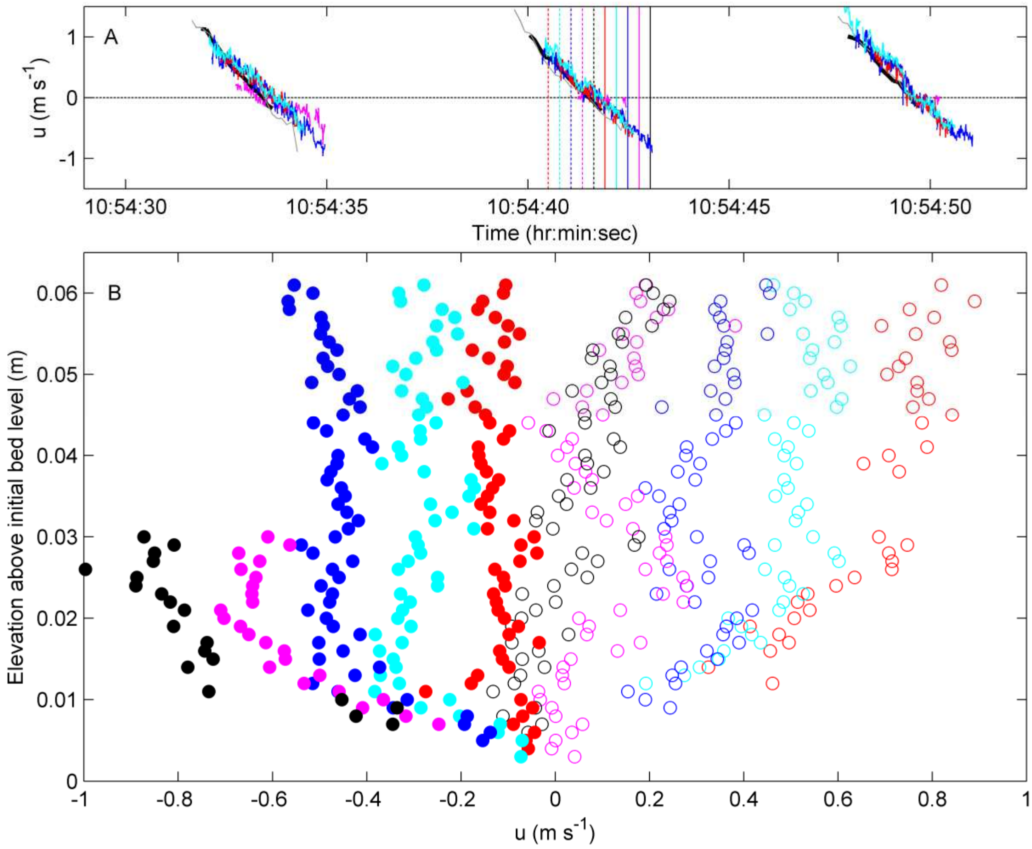


Figure 7. Example VEC data from test A2. A) Time series showing 3 swash events with colors indicating velocities from different elevations in the water column (magenta: ~0.002 m, blue: ~0.022 m, red: ~0.032 m, cyan: ~0.052 m). Corresponding EMCM velocities at ~0.06 (gray) and ~0.09 m (black) are plotted behind VEC data. B) Velocity profiles corresponding to the times indicated by the vertical lines in A. Dashed lines and open circles correspond to uprush while solid lines and filled circles correspond to backwash.

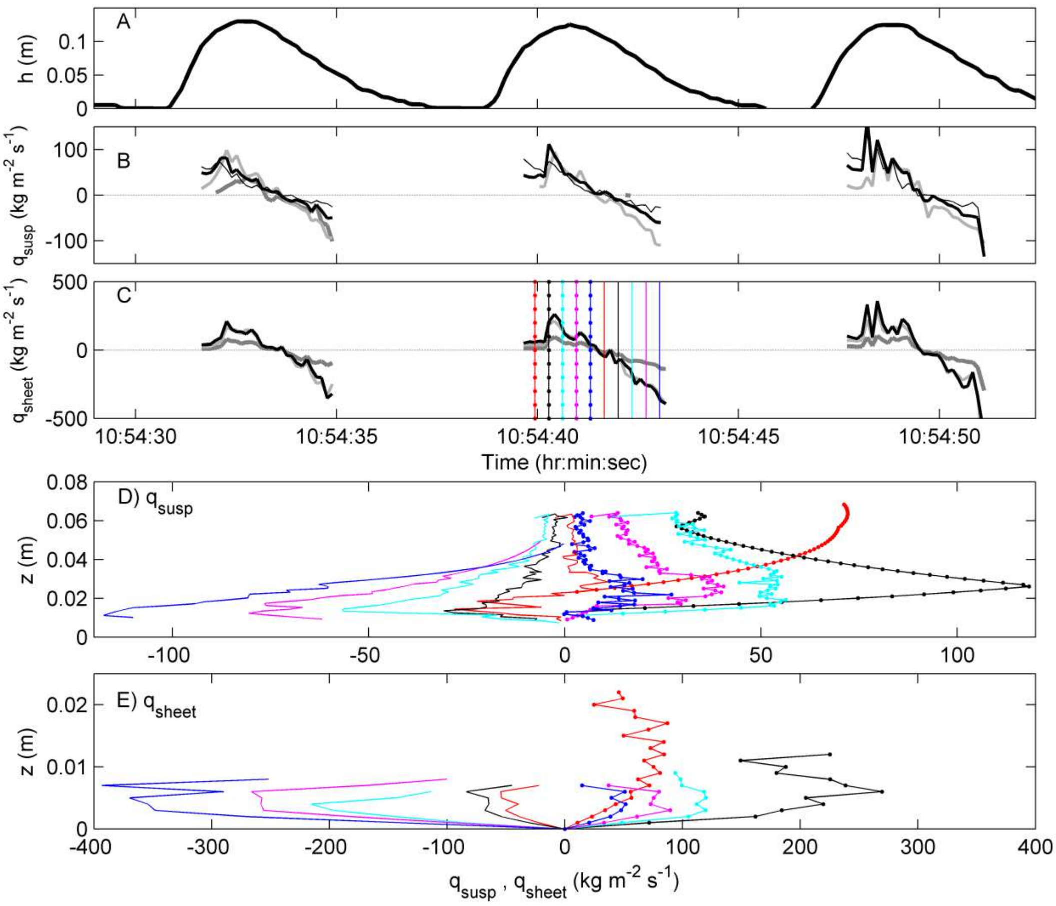


Figure 8. Example sediment fluxes from test A2. A) Water depth. B) Suspended sediment flux time series from several elevations in the water column (Thick dark grey: ~0.005 m, light grey: ~0.015 m; thick black: ~0.025 m; black: ~0.035 m). C) Sheet flow sediment flux time series from several elevations above the bed (Thick dark grey: ~0.002 m, light grey: ~0.004 m; thick black: ~0.006 m). D) Suspended sediment flux profiles corresponding to the times indicated by the vertical lines in C. E) Sheet flow sediment flux profiles corresponding to the times indicated by the vertical lines in C. For D,E dash-dot lines correspond to uprush and solid lines correspond to backwash.

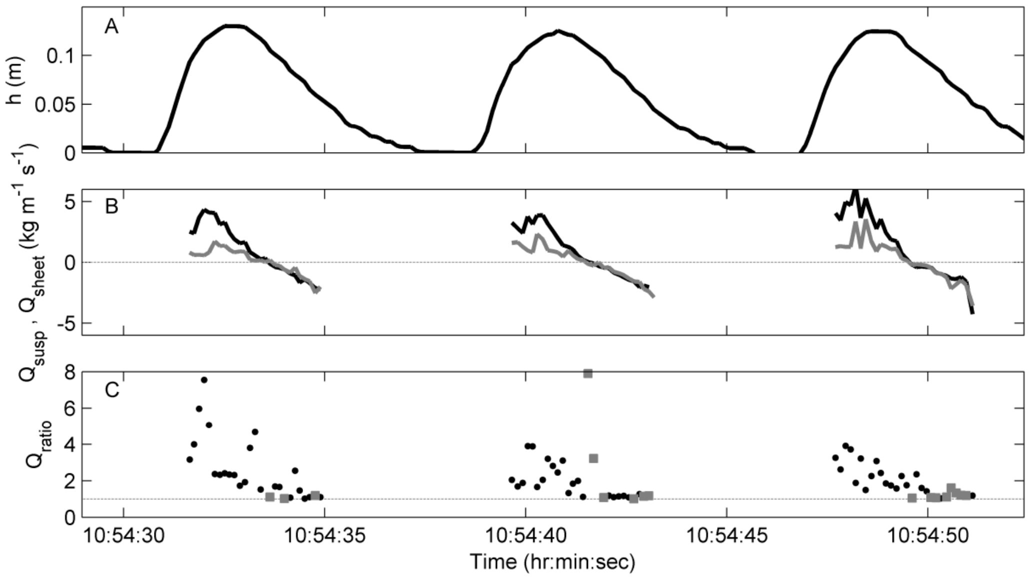


Figure 9. Example sediment transport rates for test A2. A) Water depth. B) Sediment transport rates for suspended load (black) and sheet load (grey). C) $Q_{ratio}$ relating sheet load transport to suspended load transport. Black (grey) symbols indicate suspended (sheet) load dominance. The dashed horizontal line at a $Q_{ratio}$ of 1 is where the transport modes are equivalent.

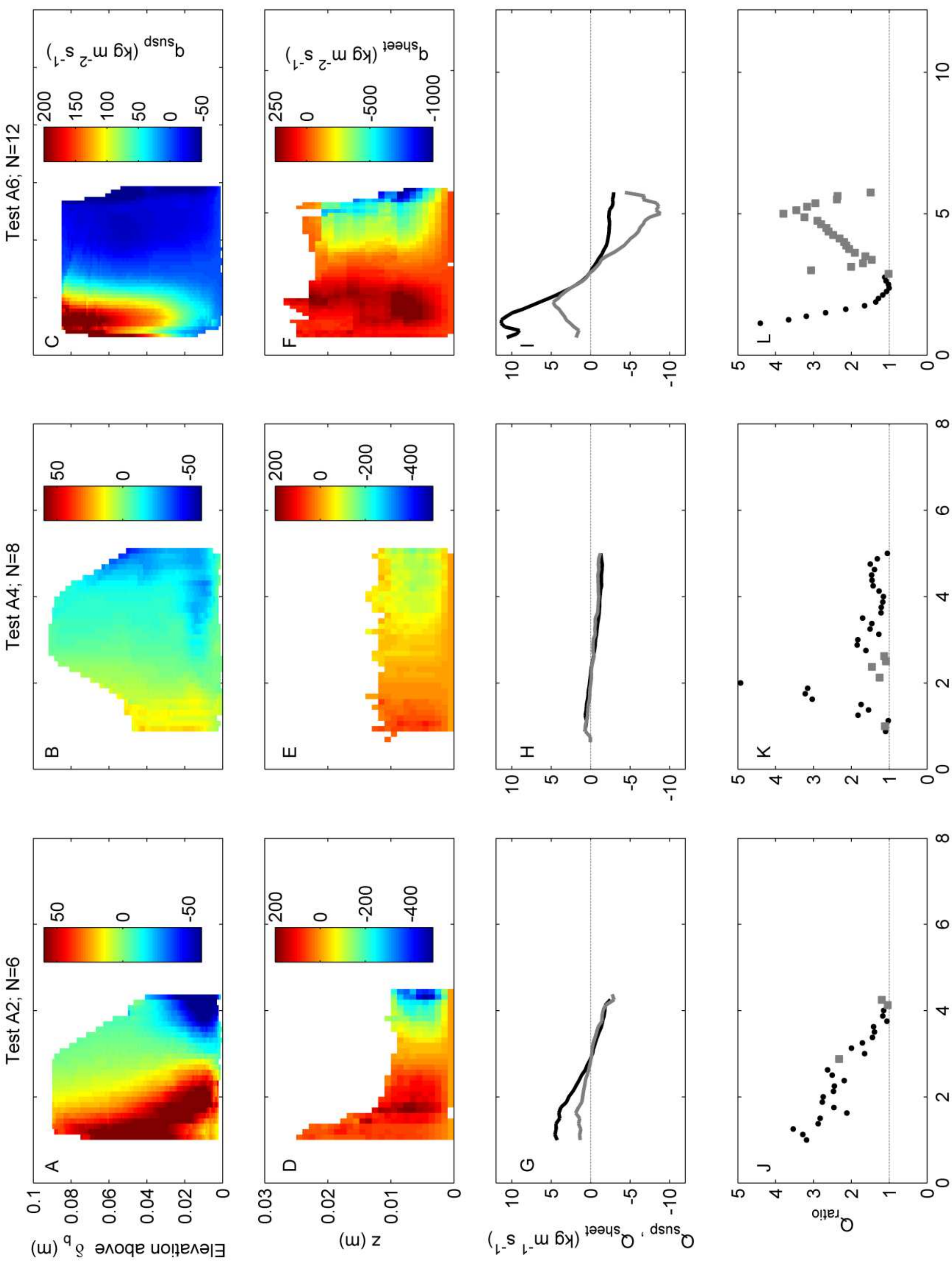

Test A2; N=6
Test A4; N=8
Test A6; N=12
Elevation above $\delta_b$ (m)
z (m)
$Q_{susp}$, $Q_{sheet}$ (kg m$^{-1}$ s$^{-1}$)
$Q_{ratio}$
$q_{susp}$ (kg m$^{-2}$ s$^{-1}$)
$q_{sheet}$ (kg m$^{-2}$ s$^{-1}$)
Time (s)
A
B
C
D
E
F
G
H
I
J
K
L

Figure 10. Ensemble average events for test A2 (left column; 6 events), A4 (middle column; 8 events) and A6 (right column; 12 events). A,B,C) Suspended sediment flux. D,E,F) Sheet flow sediment flux. Note the difference in color scale for test A6. G,H,I) Suspended (black) and sheet load (grey) transport. J,K,L) $Q_{ratio}$ as described in Figure 9.

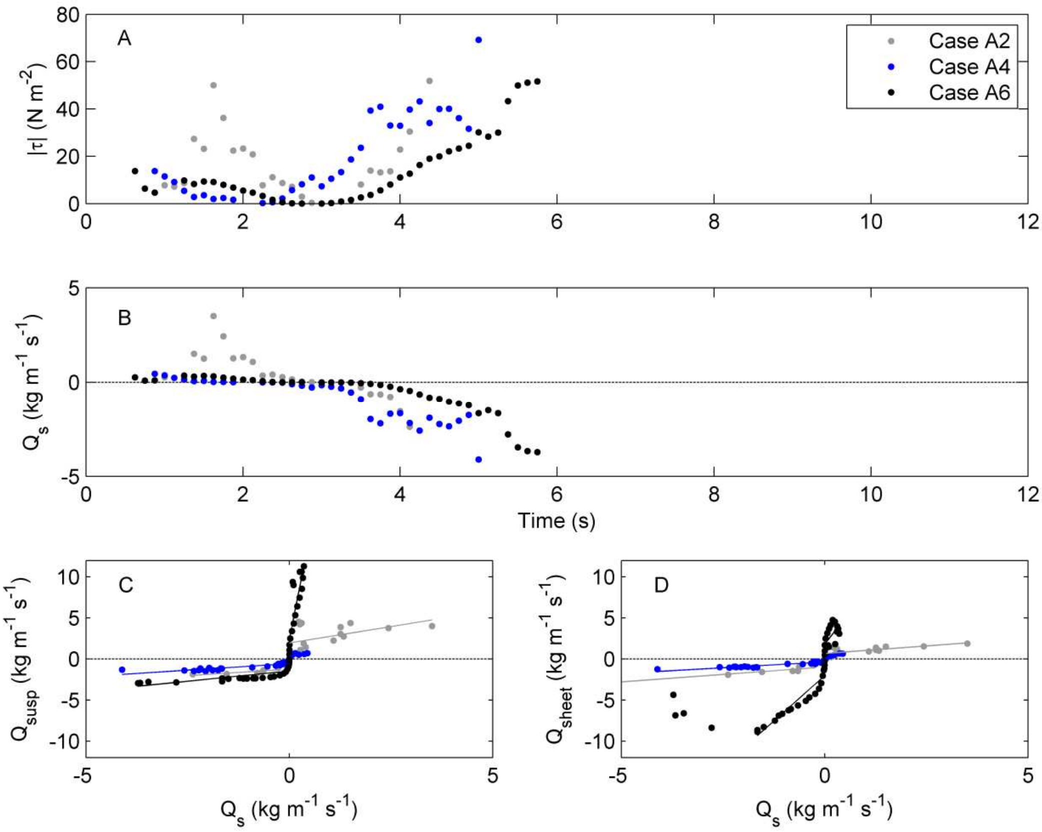


Figure 11. A) Shear stress magnitude estimates from ensemble average velocity profiles. B) sediment load transport estimate from eq. (9) setting *k* equal to unity. C) Suspended load sediment transport compared to the transport load estimate. D) Sheet load sediment transport compared to the transport load estimate. For C and D, solid lines are least squares regression fits between model and data and are calculated for uprush and backwash individually. Note that in D test A6, the regressions do not include the points less than -2 kg $m^{-1}$ $s^{-1}$ as they do not follow the trend.

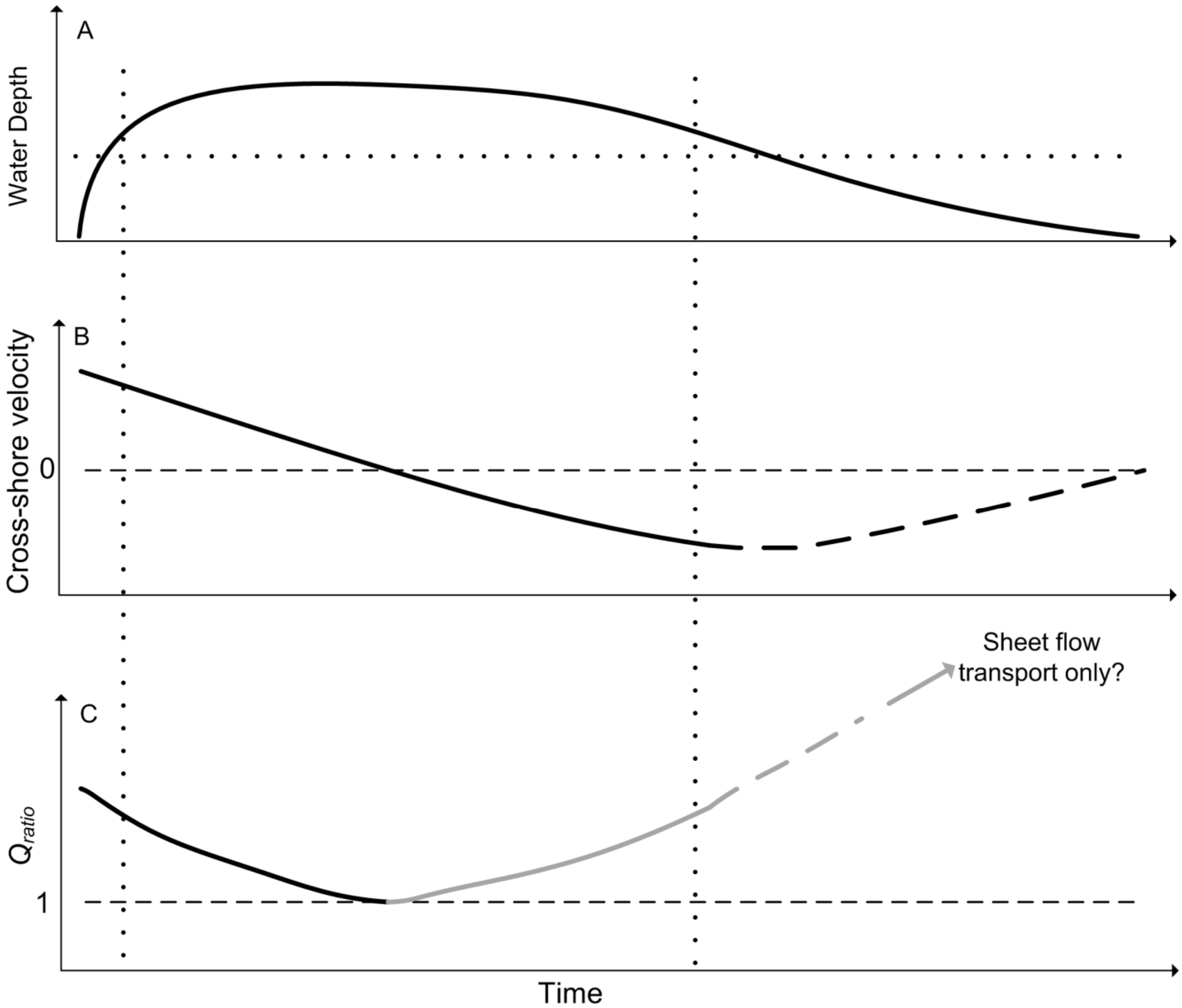


Figure 12. Schematic showing a typical water depth (A) for the 12.2 s monochromatic swash event. The cross-shore velocity with positive onshore (B). Dashed lines indicate expected velocity history for the thinning flow. The $Q_{ratio}$ (C) with suspended load dominance (black) during uprush and sheet flow dominance during backwash (gray). Dashed gray curve is the speculated relationship for the thinning flow.

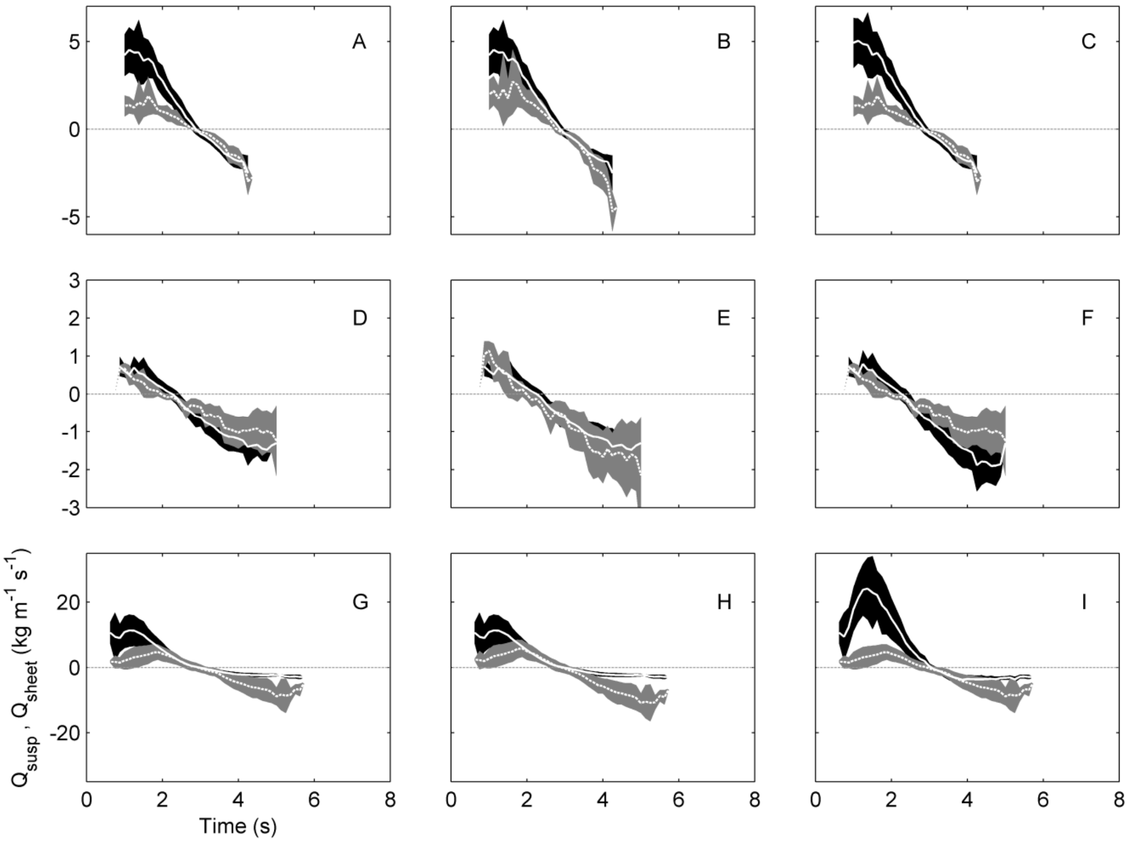


Figure 13. Sensitivity tests for sediment transport estimates. Tests A2, A4 and A6 are in rows 1 (A,B,C), 2 (D,E,F) and 3 (G,H,I) respectively. Column 1 (A,D,G) contains the original sediment transport estimates using eqs. (2-5). Column 2 (B,E,H) contains additional sheet flows sediment transport estimates by altering the sheet flow velocity profile to have a quadratic rather than linear profile. The suspended sediment transport is unchanged from the original estimate. Column 3 contains additional suspended sediment transport estimates by extrapolating the velocity and sediment concentration profiles to the free surface. The sheet flow sediment transport is unchanged from the original estimate. Black (grey) regions denote suspended (sheet flow) sediment transport rates containing the mean (white solid or dashed curves) ± 1 standard deviation. The gray horizontal line represents zero sediment transport. Axis labels for (G) apply to all axes.

Table 1. Monochromatic wave cases used in this study*.

| Case number | $H$ (m) | $T$ (s) | $h_s$ (m) | $h_l$ (m) | Local Foreshore Slope |
|---|---|---|---|---|---|
| A2 (June 12, 2012) | 0.74 | 8 | 3 | 4.3 | 1:8.9 |
| A4 (June 14, 2012) | 0.74 | 8 | 3 | 1.75 | 1:8.7 |
| A6 (June 18, 2012) | 0.74 | 12.2 | 3 | 3 | 1:6.5 |

*$H$ is the wave height; $T$ is the wave period; $h_s$ is the sea level; $h_l$ is the lagoon level.

Table 2. Transport ratios and ranges for ensemble average events*.

| Case number | $Q_{ratio}$ *(mean ± st. dev)* | *Range 25th – 75th prctile* | $Q_{ratio}$ *(mean ± st. dev)* | *Range 25th – 75th prctile* |
|---|---|---|---|---|
| A2 (June 12, 2012) | 2.34±0.94 | 1.55-2.80 | 1.52±0.70 | 1.07-2.04 |
| A4 (June 14, 2012) | 1.73±0.86 | 1.24-1.79 | 6.97±14.12 | 1.12-1.45 |
| A6 (June 18, 2012) | 2.75±1.90 | 1.12-4.41 | 2.40±0.69 | 1.95-2.92 |

*Black (gray) text denotes suspended (sheet) load dominance.

Table 3. Regression statistics ($r^2$, $k$) for the simple sediment transport model.

| Case number | Uprush $Q_{susp}$ | | Uprush $Q_{sheet}$ | | Backwash $Q_{susp}$ | | Backwash $Q_{sheet}$ | |
|---|---|---|---|---|---|---|---|---|
| | $r^2$ | $k$ | $r^2$ | $k$ | $r^2$ | $k$ | $r^2$ | $k$ |
| A2 (June 12, 2012) | 0.24 | 0.79 | 0.50 | 0.37 | 0.66 | 0.32 | 0.90 | 0.36 |
| A4 (June 14, 2012) | 0.53 | 0.76 | 0.88 | 1.33 | 0.72 | 0.31 | 0.84 | 0.28 |
| A6 (June 18, 2012) | 0.72 | 24.7 | 0.36 | 6.20 | 0.56 | 0.50 | 0.91 | 4.42 |